



Experimental Research on the Movement Patterns of Flat-Shaped Block in Debris Flows

Lei Feng^{1,2}

¹Laboratory of Mountain Hazards and Earth Surface Process, Institute of Mountain Hazards and Environment, Chinese Academy of Sciences, Chengdu, China

²University of Chinese Academy of Sciences, Beijing, China

Email: fenglei21@mails.ucas.ac.cn

How to cite this paper: Feng, L. (2024) Experimental Research on the Movement Patterns of Flat-Shaped Block in Debris Flows. *Open Access Library Journal*, 11: e11344.

<https://doi.org/10.4236/oalib.1111344>

Received: February 24, 2024

Accepted: March 25, 2024

Published: March 28, 2024

Copyright © 2024 by author(s) and Open Access Library Inc.

This work is licensed under the Creative Commons Attribution International License (CC BY 4.0).

<http://creativecommons.org/licenses/by/4.0/>



Open Access

Abstract

Geological disasters occur frequently in China, and large-scale debris flow events have caused serious threats to people's lives and property. Debris flow has the characteristics of high density and high velocity, especially the presence of large block in debris flow, which makes debris flow a great threat to engineering structures. In order to investigate the movement patterns of flat-shaped block in debris flow, a small-scale flume experiment with precise control was carried out. In the experiment, the flow characteristics of debris flow were measured by distributed sensors, and block model simulated by metal block. At the same time, the triaxial acceleration and angular velocity changes of debris flow block were measured by an embedded inertial measurement unit (IMU). The experimental results show that the movement patterns of block in debris flow is mainly represented by sliding and rotating on the flow plane, and the movement pattern is closely related to the solid volume concentration of debris flow and the density of block. The higher the solid volume concentration and the higher the density of the block, the smaller the peak value and amplitude of the acceleration and acceleration of the block, and the block's movement pattern tends to slide.

Subject Areas

Geophysics

Keywords

Flat Block, Debris Flow, Flume Experiment, IMU

1. Introduction

Debris flows originating from mining activities represent frequent geological ca-

lamities in mountainous regions and mining locales, invariably resulting in significant human casualties and substantial property damage [1]. The nature of these mine-related debris flows is intricately tied to the composition of the slag. Notably, when waste slag comprises schist and phyllite, the propensity for debris flow formation is notably heightened. The specter of mine debris flow poses a substantial and undeniable peril to the execution of mining projects. The formidable presence of large block within debris flows underpins their immense destructive potential. Thus, efforts directed toward the prevention and mitigation of debris flow during engineering endeavors necessitate a laser focus on the influence exerted by these colossal boulders, with the overarching objective of minimizing the financial ramifications ensuing from debris flow disasters.

Within the context of debris flows, flat block emerge as a distinctive particulate variant [2]. Their distinctive morphological attributes dictate that their dynamics and behavior within debris flows may diverge from those observed in other particles. Consequently, this study endeavors to undertake a comprehensive investigation into the movement dynamics of flat block within debris flows.

The investigation into the dynamics of block movement within debris flows holds paramount research significance, particularly concerning the design and implementation of engineering protective measures [3]. While extant literature predominantly focuses on elucidating the impact of block on protective structures [2] [4], scant attention has been afforded to comprehensively studying their intricate movement patterns within the context of debris flows. Unlike the movement of block within transparent fluids, which lends itself to direct observation [5], the opaque nature of debris flows necessitates the utilization of internally embedded inertial measurement unit (IMU) for accurate assessment and analysis [6].

This study employs flume experiments to meticulously investigate the movement patterns exhibited by flat block within debris flows. Employing a multifaceted approach, it integrates the utilization of triaxial load cells, pore water pressure sensors, and ultrasonic sensors to meticulously capture and quantify the flow characteristics inherent in debris flows. Additionally, the study leverages embedded IMU sensors to meticulously measure the three-dimensional motion of block within the flow. The purpose is to conduct a preliminary study on the movement patterns of blocks in debris flow, and pave the way for the next step of predicting the travel distance and deposition mode of large rocks in debris flows.

2. Experimental Setup

2.1. Flume

The experimental setup utilizes a small-scale flume (**Figure 1**) to replicate the flow dynamics of debris flows and their interaction with structural elements [7] [8]. This flume configuration comprises two distinct sections characterized by varying slopes and lengths: an upstream acceleration section and a downstream

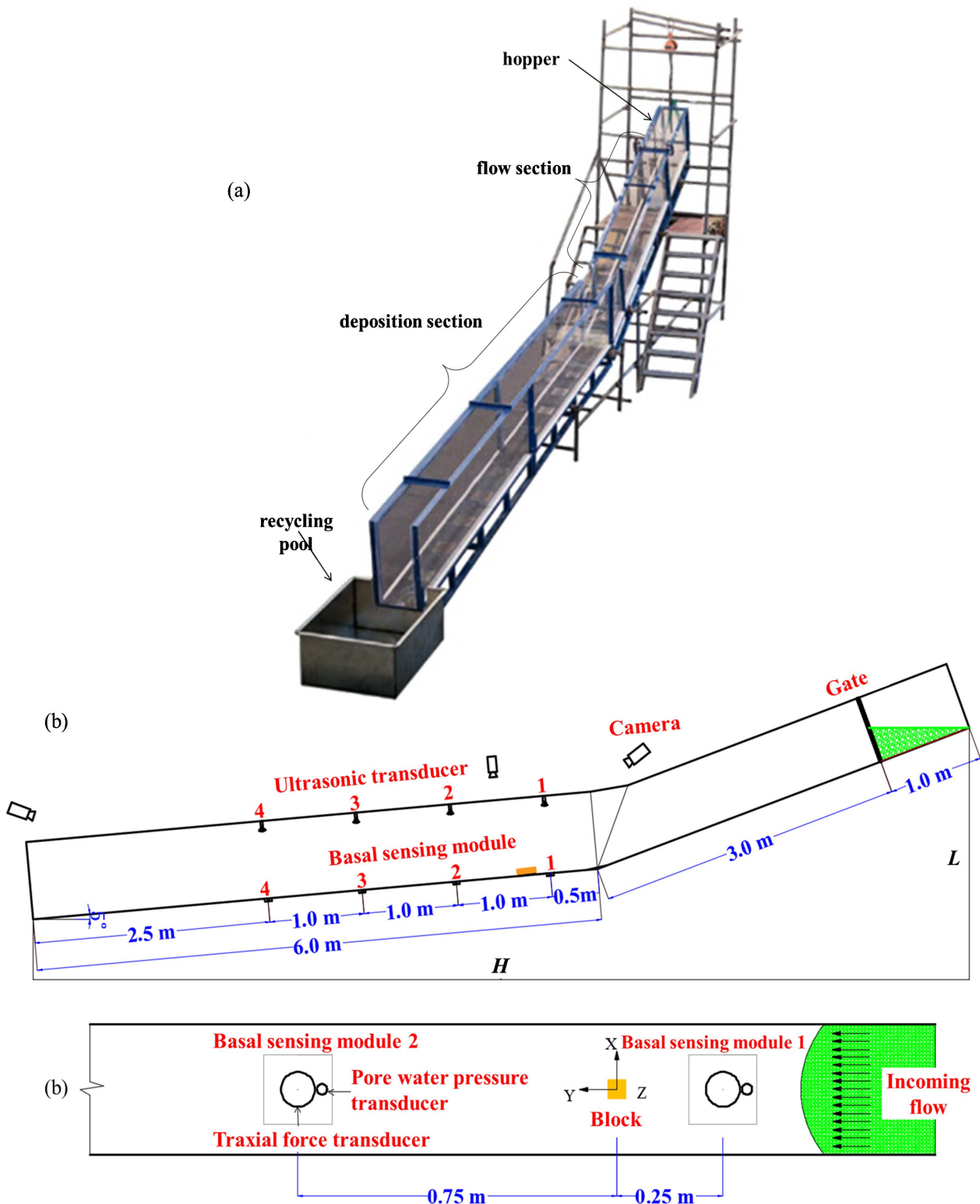


Figure 1. Flume setup (a) Photo of small-scale flume; (b) side view; (c) top view.

deposition section. The slopes are inclined at angles of 25° and 5°, respectively. The upstream section spans 3 m in length, while the downstream counterpart extends over 6 m. The entire flume boasts a width of 0.3 m (Figure 1).

2.2. Material

In the simulation of debris flow, the solid concentration is represented by single-particle-size transparent glass beads, each measuring 0.6 mm in diameter and possessing a density of 2540 kg/m³. The liquid phase consists of a blend of glycerin and water. The concentration of debris flow in this experimental setup varies across three levels: 45%, 50%, and 53%. By modulating the concentration of the solid concentration, the debris flow can exhibit different Froude numbers (Fr) and liquefaction param (λ). The total volume of debris flow released during the experiment amounts to 50 L, with a density ranging between 1772.8 kg/m³ and 1884.0 kg/m³.

2.3. Instrumentation

A series of basal sensing modules is strategically positioned at the base of the entire flume, as illustrated in **Figure 1**. Each module incorporates a triaxial load cell and a pore pressure sensor, as depicted in **Figure 2**, tasked with measuring the normal stress, shear stress, and pore water pressure at the bottom, respectively. Positioned directly above each basal sensing module is an ultrasonic sensor (**Figure 1**), facilitating the measurement of debris flow depth at the corresponding module. The data acquisition system employed enables synchronous capture of all sensor signals, with a sampling frequency set at 500 Hz. Furthermore, three DV cameras are strategically mounted atop the flume to capture the entire process from diverse perspectives, as delineated in **Figure 1**.

2.4. Block Model

The block model is crafted from stainless steel, boasting a density of 7800 kg/m³. Featuring a hollowed-out center, the metal block maintains structural symmetry, ensuring uniformity in its design. Block with densities of 2700 kg/m³ and 4500 kg/m³ are attainable, each possessing relative densities of 1.5 and 2.5 when compared to the debris flow. These blocks are meticulously fashioned into dimensions of 40 × 40 × 10 mm m³.

Embedded within the block model is an inertial measurement unit (IMU), as depicted in **Figure 3**. This module is equipped with its own power supply and

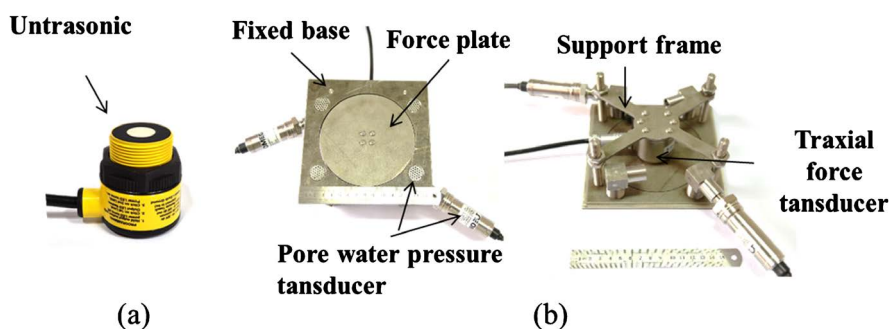


Figure 2. Photo of sensors in flume test: (a) ultrasonic sensor; (b) basal sensing module consisting of a triaxial load cell and a pore water pressure sensor.

storage capabilities, facilitating operational longevity of 5 - 6 hours. With a sampling frequency reaching 200 Hz, the module adeptly measures the three-axis acceleration and angular velocity of the block, crucial for delineating the specific movement patterns exhibited by block under the influence of the debris flow [7] [9]. The sensor boasts an acceleration range of ± 16 g, with an impressive accuracy of 0.0005 g/LSB. Additionally, it features an angular velocity measurement range of $\pm 2000^\circ/\text{s}$, coupled with an accuracy of 0.061 ($^\circ/\text{s}$)/LSB.

Prior to commencing the experiment, the inertial measuring unit is activated for data collection, and the block undergoes waterproofing procedures. Positioned between basal sensing modules 1 and 2, at a distance of 0.75 m from the downstream corner of the flume and 0.25 m from basal sensing module 1 (Figure 1). This placement not only subjects the block to the continuous, steady impact of debris flow, but also facilitates meticulous monitoring of debris flow characteristics surrounding the block.

2.5. Test Program

To scrutinize the impact of debris flow regime and block density on block movement patterns, a comprehensive set of experiments was meticulously conducted, comprising six distinct configurations achieved through variations in solid volume concentration and block density within the debris flow. The test program is delineated in Table 1.

3. Experimental Results and Analysis

The test program entails setting predefined solid volume concentration levels for

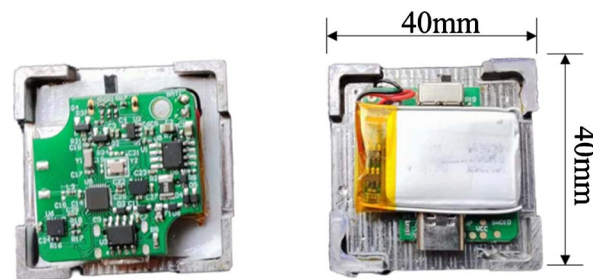


Figure 3. Photo of Inertial Measuring Unit (IMU) inside the block model.

Table 1. Test program.

ID	Concentration (%)	Debris-flow density (kg/m^3)	Blok density (kg/m^3)
45 - 1.5	45	1772.8	2700
45 - 2.5	45	1772.8	4500
50 - 1.5	50	1839.4	2700
50 - 2.5	50	1839.4	4500
53 - 1.5	53	1884.0	2700
53 - 2.5	53	1884.0	4500

various debris flows along with the density specifications for the block model. Measurements encompass triaxial acceleration and angular velocity of block within the debris flow, as well as param such as flow speed, flow depth, and internal stress (including normal stress, shear stress, and pore water pressure) within the debris flow. Subsequently, based on these measurements, calculations are performed to determine the Froude number and liquefaction ratio of the debris flow. These comprehensive analyses enable the elucidation of the impacts of debris flow characteristics and block density on the movement patterns of block within debris flows. These test results are summarized in **Table 2** for further analysis and interpretation.

3.1. Debris-Flow Mobility

Debris flows tend to deposition in areas where the downstream slope exhibits gentleness [8] [10]. With a consistent release volume of 50 L in each experiment, the formation of depositions was observed in simulated debris flows. Subsequently, the height of the deposition area was meticulously measured at intervals of 0.5 m along the deposition zone, facilitating the construction of deposition curves, as depicted in **Figure 4**.

Through comparative analysis of experimental outcomes, notable distinctions emerge: depositions of low-solid-concentration debris flows exhibit greater length but smaller thickness, whereas those high-solid-concentration debris flows deposition-length reduced area yet increased thickness. To quantitatively assess debris flow mobility, the ratio of horizontal flow distance (L) to vertical drop height (H), denoted as L/H , is employed as a metric [11] [12]. By plotting a relationship curve between solid volume concentration and mobility, as illustrated

Table 2. Test results.

ID	relative density	front velocity (m/s)	flow depth (kg/m ³)	Deposition length (m)	Froude number Fr	Liquefaction ratio λ	mobility L/H
45 - 1.5	1.5	1.98	0.036	4.05	3.33	0.85	4.17
45 - 2.5	1.5	2.08	0.039	4.10	3.35	0.73	4.19
50 - 1.5	1.5	1.29	0.046	2.73	1.92	0.72	3.61
50 - 2.5	2.5	1.09	0.048	2.21	1.59	0.65	3.37
53 - 1.5	2.5	0.06	0.050	1.29	0.09	0.66	2.90
53 - 2.5	2.5	0.07	0.048	1.06	0.10	0.61	2.78

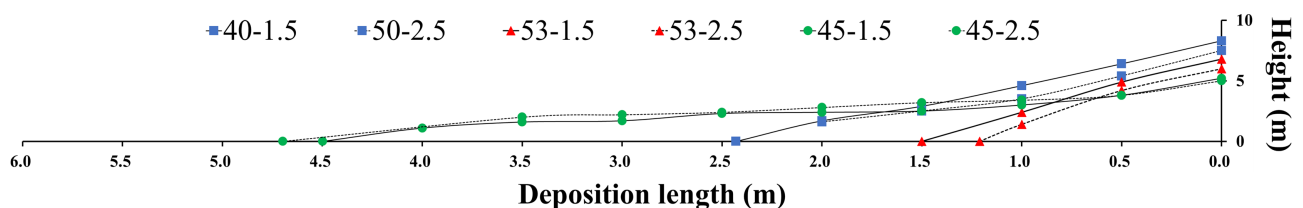


Figure 4. Photo of Inertial Measuring Unit (IMU) inside the block model.

in **Figure 5**, a discernible trend emerges: an increase in solid-phase concentration correlates with a concomitant decrease in debris flow deposition length and L/H ratio. This observation underscores the notion that, for debris flows of identical volumes, heightened solid concentration engenders a diminishment in mobility.

3.2. Debris-Flow Regime

The basal sensing modules and ultrasonic sensors are systematically positioned along the deposition area, with measurements taken at intervals of 0.5 m, 1.5 m, 2.5 m, and 3.5 m within the deposition zone. These measurements encompass normal stress, shear stress, and pore water pressure recorded by the four basal sensing modules, along with flow depth measured by the top ultrasonic sensor, as delineated in **Figure 6**. Effective data collection is contingent upon sensor placement in areas directly traversed by the debris flow. Consequently, in scenarios where debris flow with a 45% solid concentration exhibits optimal mobility, all four positions yield responsive sensor readings (**Figure 6(a1)**). Conversely, in experiments involving debris flow with a 53% solid concentration, only basal sensing module 1 and ultrasonic 1 register valid data (**Figure 6(c1)**).

Flow velocity of the debris flow is ascertained via analysis of images captured by the camera. Subsequently, leveraging the flow depth data obtained from the ultrasonic sensor, the Froude number of the debris flow can be meticulously calculated [13]:

$$Fr = \frac{v}{\sqrt{gh \cos \theta}} \quad (1)$$

where v is the flow velocity, h is the flow depth, g is the gravity acceleration, and θ is the slope.

The degree of liquefaction is the ratio of pore water pressure and normal stress in the debris flow (**Figure 6(a2)**) [14] [15]:

$$\lambda = \frac{\text{Pore water pressure}}{\text{Normal stress}} \quad (2)$$

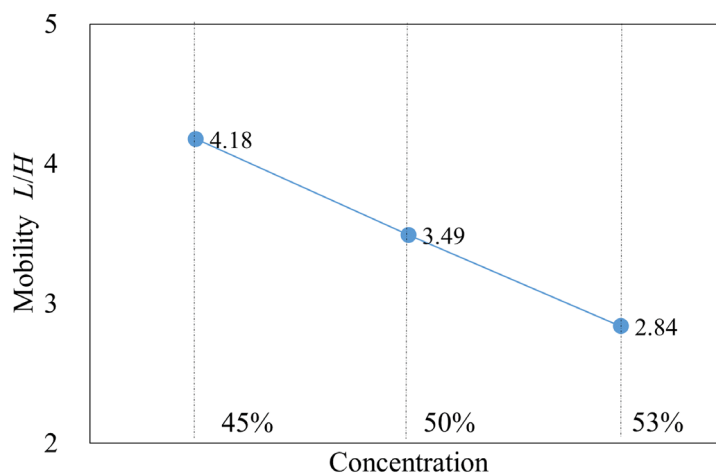


Figure 5. Relationship between debris-flow solid volume concentration and mobility.

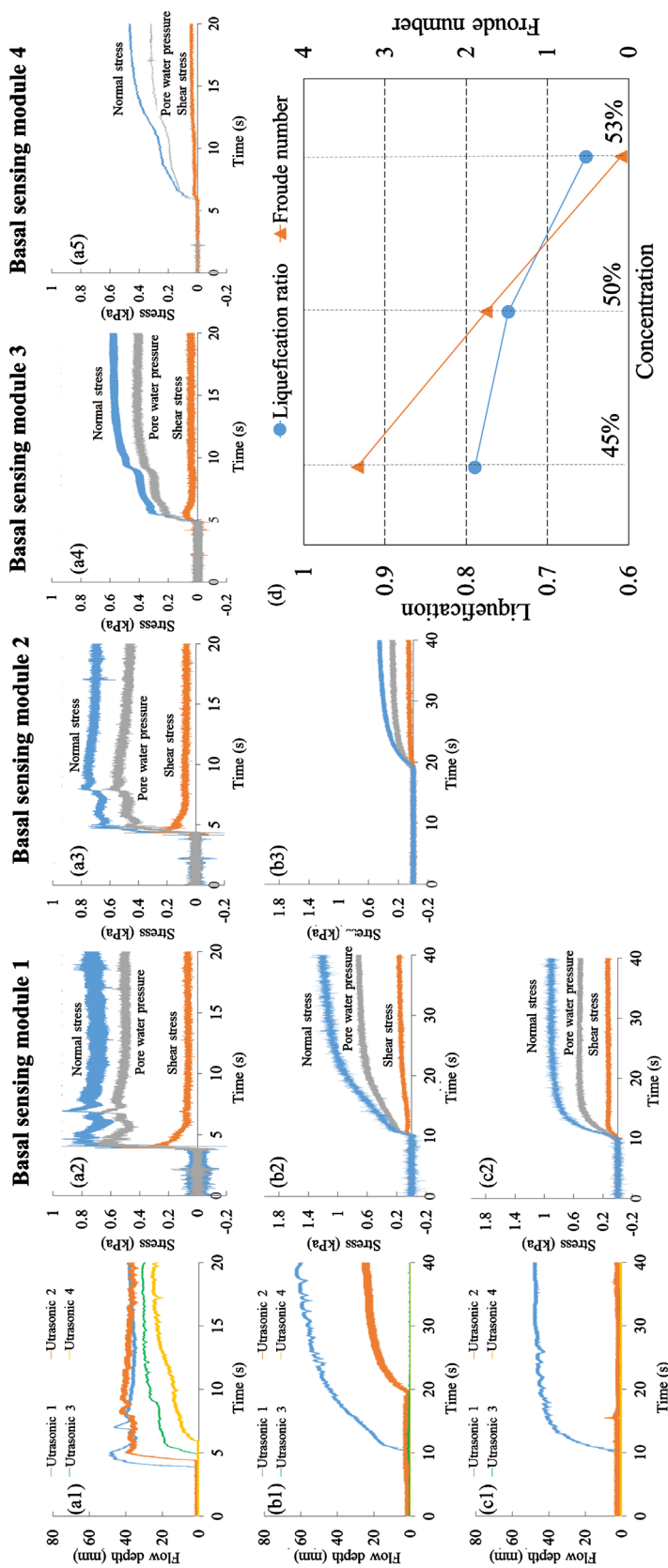


Figure 6. Data of the basal sensing modules and ultrasonic sensor (a) test 45 - 1.5; (b) test 50 - 2.5; (c) test 53 - 2.5; (d) relationships between solid volume concentration and liquefaction ratio and Froude number.

In the experimental setup, alterations in the Froude number and liquefaction degree were solely achieved by varying the solid volume concentration of the debris flow. As the solid volume concentration increased, both the Froude number and the liquefaction degree exhibited a discernible decreasing trend, as illustrated in **Figure 6(d)**. The liquefaction ratio ranged from a maximum value of 0.85 to a minimum of 0.61, while the Froude number spanned from a maximum of 3.35 to a minimum of 0.09, as detailed in **Table 2**. Given the relatively diminutive volume of block in comparison to the experimentally simulated debris flow, their influence on the Froude number and liquefaction degree of the debris flow remains negligible.

3.3. Block Movement Patterns

The three-axis acceleration and three-axis angular velocity results, as measured by the IMU, are delineated in **Figure 7**. Here, the x-axis, y-axis, and z-axis correspond to the pitch angle, roll angle, and heading angle, respectively.

While theoretically, integrating the acceleration in the direction of the block's movement enables derivation of its velocity, and subsequent integration yields displacement, practical integration often entails significant error [6]. Consequently, this study exclusively focuses on analyzing the instantaneous motion state of the block as measured by IMU.

Theoretically, the impact force of debris flow can be expressed as [16]:

$$F = \alpha \rho v^2 \quad (3)$$

where α represents the empirical coefficient, ρ denotes the density of the debris flow, and v signifies the flow velocity of the debris flow. The uniformly stirred debris flow is released through the gate of the upstream hopper, culminating in the formation of a uniform and stable flow. Upon contact with the block, the debris flow front imparts impact upon them, thereby causing a sudden increase in the y-axis acceleration of the block, as depicted in **Figure 7**.

Throughout the movement process, gravitational influence ensures that the acceleration in the z-axis direction remains constant. This signifies that, during movement, the positive direction of the z-axis of the block remains unaltered, indicating non-rotational movement with the block rotating solely around the z-axis within the xoy plane. Upon cessation of debris flow movement, the relative magnitudes of acceleration values along the x-axis and y-axis undergo reversal, as depicted in **Figure 7(a)**. This indicates a 90° rotation of the block angle post-debris deposition compared to the initial angle.

Furthermore, as illustrated in **Figure 7(b)**, following the cessation of debris flow movement and deposition, the x-axis and y-axis of the sensor exhibit identical accelerations, indicating a 45° rotation around the z-axis relative to the initial position. Additionally, in **Figure 7(e)**, the angular velocity of the block during movement displays minimal fluctuation amplitude, with the three-axis acceleration post-deposition mirroring that of the initial state. This observation implies that the block solely undergoes translational sliding without rotational motion.

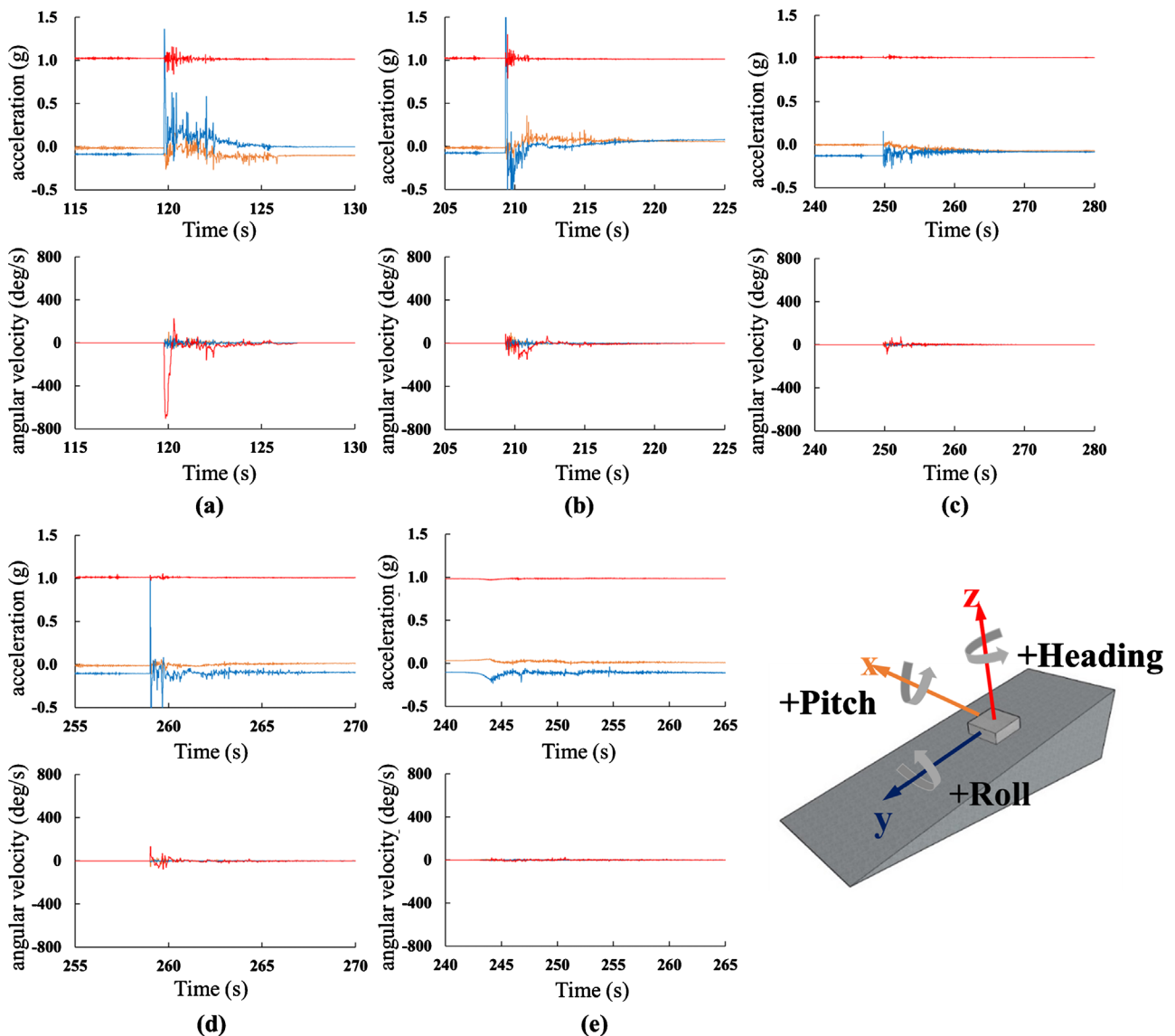


Figure 7. Measurement data of IMU (a) test 45 - 1.5; (b) test 50 - 1.5; (c) test 53 - 1.5; (d) test 45 - 2.5; (e) test 50 - 2.

During the movement of the block, there exists a propensity for forward falling under the compressive influence of the debris flow. In Experiment 50 - 2.5 (Figure 7(e)), where the density of the block is 2.5 times that of the debris flow and the mobility of the debris flow is poor, the block do not undergo vigorous rotation within the xoy plane but rather slide slowly in the direction of flow. Notably, the acceleration of the block in the flow direction (y-axis) continues to increment in the negative direction, indicative of a change in the pitch angle of the block.

While there is a tendency for the block to pitch forward during movement, flipping does not occur. This can be attributed to the flat shape of the block and its height-to-length ratio of 1:4. Given this configuration, the block encounters difficulty in toppling over, thereby necessitating a sliding pattern of movement. It's worth noting that when the height-to-length ratio of the block approaches

1:1, the block may transition to a rolling pattern of movement (See **Figure 8**).

3.4. Effects of Debris Flow Regime and Mobility on Block Movement Patterns

During the sliding process of the block, frictional collisions between the block and the bottom of the flume induce fluctuations in three-axis acceleration and angular velocity. Notably, the z-axis direction experiences the most significant change in angular velocity, while the y-axis direction exhibits the most noticeable acceleration variation. The amplitude of these fluctuations correlates with the solid volume concentration of the debris flow. Debris flows characterized by low solid volume concentration demonstrate heightened dynamics and accelerated flow velocity. Consequently, the impact force exerted by block on the debris flow is amplified, resulting in more pronounced fluctuations in both acceleration and angular velocity of the block.

Moreover, these fluctuations in acceleration and angular velocity serve as indicative markers of the duration of the entire movement process. For instance, during experiments involving the pushing of block with a 53% solid-phase debris flow, fluctuations in acceleration and angular velocity persisted for approximately 20 s. Conversely, in experiments with 45% solid-phase debris flow, these fluctuations were limited to a mere 5 s. This discrepancy underscores the profound impact of debris flow mobility on the duration of block movement. In this study's small flume experiments, higher solid volume concentration in debris flows of identical volumes corresponds to diminished mobility and consequently prolonged flow times.

3.5. Effect of Block Density on Movement Patterns

Comparative analysis of the impact of block density on movement patterns reveals discernible distinctions. High-density block exhibit a smaller peak acceleration along the y-axis (flow direction) upon initial impact by a debris flow, as depicted in **Figure 9(a)**, in contrast to low-density block. This discrepancy can be attributed to the greater inertia of high-density block, rendering them more resistant to displacement by debris flow and thus resulting in smaller accelerations.

Furthermore, during the movement of high-density block within the debris flow, the peak angular velocity along the z-axis (xoy plane) is also observed to be

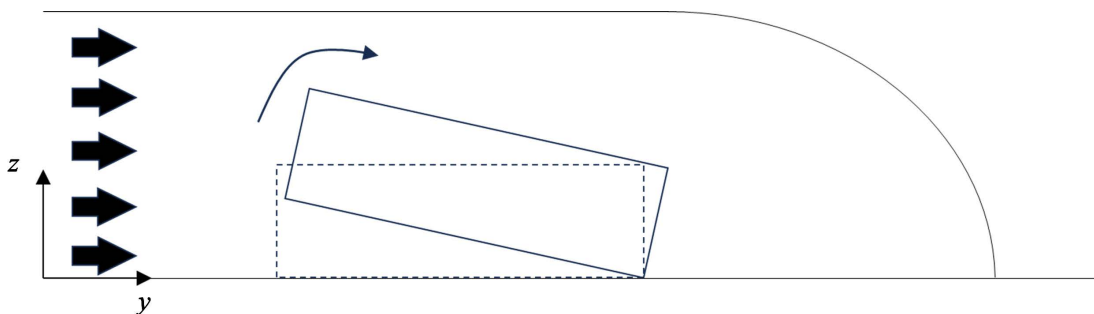


Figure 8. Schematic diagram for block flipping.

smaller compared to low-density block, as illustrated in **Figure 9(b)**. This observation further underscores the more stable movement pattern of high-density block, with fluctuations in both acceleration and angular velocity markedly reduced in comparison to low-density block.

Moreover, as depicted in **Figure 7**, high-density block exhibits a movement pattern characterized by enhanced stability during motion, with a tendency towards sliding.

4. Conclusions

In summary, this study delves into the movement patterns of flat block within debris flows, examining the influence of varying solid volume concentration and block density on block movement. The following key findings emerge:

1) The mobility and flow behavior of debris flows are intimately linked to their solid volume concentration. Debris flows with lower solid volume concentration exhibit superior mobility, resulting in larger deposition areas, higher Froude numbers, and greater degrees of liquefaction.

2) Flat block within debris flows primarily undergo rotational sliding within the xoy plane, with rolling and jumping movements being negligible. Notably, in experiments with highly fluid debris flows, block experience maximum acceleration upon impact, accompanied by violent fluctuations in three-axis acceleration and angular velocity. Conversely, in less fluid debris flows, acceleration peaks are minimal, with correspondingly reduced fluctuations in acceleration and angular velocity.

3) High-density block present greater resistance to movement compared to low-density counterparts. Upon impact, high-density block exhibit smaller acceleration amplitudes, with corresponding reductions in three-axis acceleration and angular velocity fluctuations during movement. The movement pattern of high-density block in debris flows with high solid volume concentration is characterized by sluggish movement, with block inclined to tilt forward.

4) When designing protective structures for mining projects, careful consideration should be given to the impact of flat block, such as schist and phyllite, within low-solid debris flows. Structural design should account for factors such

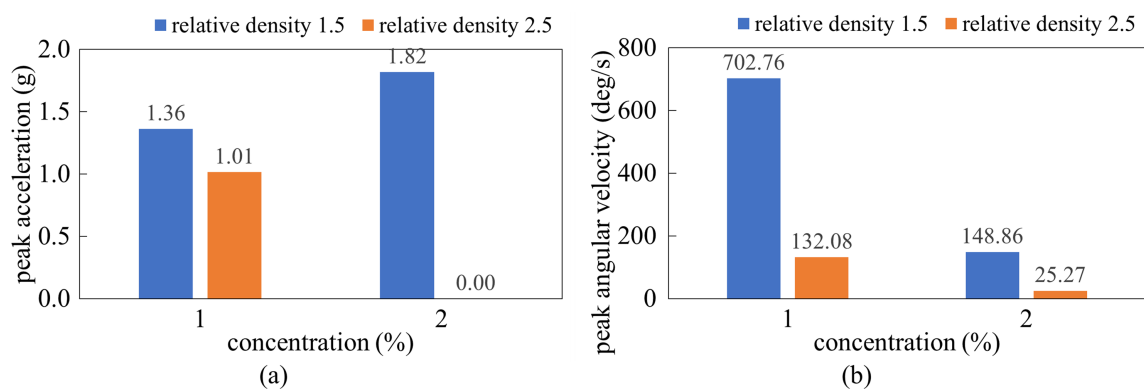


Figure 9. Relationship between block density and (a) peak acceleration and (b) peak angular velocity.

as impact direction, velocity, and potential impact force of the debris flow. Through strategic structural design and layout, the impact force on structures can be mitigated, thereby enhancing overall structural resilience.

Presently, the ongoing investigation merely initiates a preliminary examination into the motion characteristics of planar blocks within debris flows. The experimentally replicated debris flow scenarios and block models represent idealized conditions, thus deviating from real-world scenarios to a certain extent. Future research endeavors will necessitate a comprehensive analysis of block movement patterns.

Conflicts of Interest

The author declares no conflicts of interest.

References

- [1] Dowling, C.A. and Santi, P.M. (2013) Debris Flows and Their Toll on Human Life: A Global Analysis of Debris-Flow Fatalities from 1950 to 2011. *Natural Hazards*, **71**, 203-227. <https://doi.org/10.1007/s11069-013-0907-4>
- [2] Si, G.-W., Chen, X.-Q., Chen, J.-G., Tang, J.-B., Zhao, W.-Y. and Jin, K. (2022) The Impact Force of Large Boulders with Irregular Shape in Flash Flood and Debris Flow. *KSCE Journal of Civil Engineering*, **26**, 4276-4289. <https://doi.org/10.1007/s12205-022-0680-6>
- [3] Zhao, L., He, J.W., Yu, Z.X., Liu, Y.P., Zhou, Z.H. and Chan, S.L. (2020) Coupled Numerical Simulation of a Flexible Barrier Impacted by Debris Flow with Boulders in Front. *Landslides*, **17**, 2723-2736. <https://doi.org/10.1007/s10346-020-01463-x>
- [4] Chehade, R., Chevalier, B., Dedecker, F., Breul, P. and Thouret, J.-C. (2022) Effect of Boulder Size on Debris Flow Impact Pressure Using a CFD-DEM Numerical Model. *Geosciences*, **12**, 188. <https://doi.org/10.3390/geosciences12050188>
- [5] Nandasena, N.A.K. and Tanaka, N. (2013) Boulder Transport by High Energy: Numerical Model-Fitting Experimental Observations. *Ocean Engineering*, **57**, 163-179. <https://doi.org/10.1016/j.oceaneng.2012.09.012>
- [6] Harding, M., Fussell, B.K., Gullison, M., Benoît, J. and De Alba, P. (2014) Design and Testing of a Debris Flow “Smart Rock”. *Geotechnical Testing Journal*, **37**, 769-785. <https://doi.org/10.1520/GTJ20130172>
- [7] Caviezel, A. and Gerber, W. (2018) Brief Communication: Measuring Rock Decelerations and Rotation Changes during Short-Duration Ground Impacts. *Natural Hazards and Earth System Sciences*, **18**, 3145-3151. <https://doi.org/10.5194/nhess-18-3145-2018>
- [8] Baselt, I., de Oliveira, G.Q., Fischer, J.-T. and Pudasaini, S.P. (2022) Deposition Morphology in Large-Scale Laboratory Stony Debris Flows. *Geomorphology*, **396**, Article 107992. <https://doi.org/10.1016/j.geomorph.2021.107992>
- [9] Curley, E.A.M., Valyrakis, M., Thomas, R., Adams, C.E. and Stephen, A. (2021) Smart Sensors to Predict Entrainment of Freshwater Mussels: A New Tool in Freshwater Habitat Assessment. *Science of the Total Environment*, **787**, Article 147586. <https://doi.org/10.1016/j.scitotenv.2021.147586>
- [10] Zhou, W., Fang, J., Tang, C. and Yang, G. (2019) Empirical Relationships for the Estimation of Debris Flow Runout Distances on Depositional Fans in the Wenchuan Earthquake Zone. *Journal of Hydrology*, **577**, Article 123932.

-
- <https://doi.org/10.1016/j.jhydrol.2019.123932>
- [11] Gao, L., Zhang, L.M., Chen, H.X., Fei, K. and Hong, Y. (2021) Topography and Geology Effects on Travel Distances of Natural Terrain Landslides: Evidence from a Large Multi-Temporal Landslide Inventory in Hong Kong. *Engineering Geology*, **292**, Article 106266. <https://doi.org/10.1016/j.enggeo.2021.106266>
- [12] Davies, T.R. and McSaveney, M.J. (1999) Runout of Dry Granular Avalanches. *Canadian Geotechnical Journal*, **36**, 313-320. <https://doi.org/10.1139/t98-108>
- [13] Iverson, R.M. (1997) The Physics of Debris Flows. *Reviews of Geophysics*, **35**, 245-296. <https://doi.org/10.1029/97RG00426>
- [14] Iverson, R.M., George, D.L., Allstadt, K., Reid, M.E., Collins, B.D., Vallance, J.W., Schilling, S.P., Godt, J.W., Cannon, C.M., Magirl, C.S., Baum, R.L., Coe, J.A., Schulz, W.H. and Bower, J.B. (2015) Landslide Mobility and Hazards: Implications of the 2014 Oso Disaster. *Earth and Planetary Science Letters*, **412**, 197-208. <https://doi.org/10.1016/j.epsl.2014.12.020>
- [15] Jakob, M., Hungr, O., Sassa, K. and Wang, Gh. (2005) Mechanism of Landslide-Triggered Debris Flows: Liquefaction Phenomena Due to the Undrained Loading of Torrent Deposits. *Debris-Flow Hazards and Related Phenomena*, 81-104.
- [16] Cui, P., Zeng, C. and Lei, Y. (2015) Experimental Analysis on the Impact Force of Viscous Debris Flow. *Earth Surface Processes and Landforms*, **40**, 1644-1655. <https://doi.org/10.1002/esp.3744>